Singlet Energy Transfer in Porphyrin-Based Donor−Bridge−Acceptor Systems: Interaction between Bridge Length and Bridge Energy

Karin Pettersson,[†] Alexander Kyrychenko,[†,‡] Elin Rönnow,[†] Thomas Ljungdahl,[§] Jerker Mårtensson,[§] and Bo Albinsson*[,†]

Departments of Chemical and Biological Engineering, Physical Chemistry, and Organic Chemistry, Chalmers University of Technology, SE-412 96 Göteborg, Sweden

Received: July 12, 2005; In Final Form: October 14, 2005

Singlet excitation energy transfer is governed by two donor−acceptor interactions, the Coulombic and exchange interactions giving rise to the Förster and Dexter mechanisms, respectively, for singlet energy transfer. In transfer between colliding molecules or between a donor (D) and acceptor (A) connected in donor−bridge−acceptor (D−B−A) system by an inert spacer (B), the distinction between these two mechanisms is quite clear. However, in D−B−A systems connected by a π-conjugated bridge, the exchange interaction between the donor and acceptor is mediated by the virtual low-lying excited states (unoccupied orbitals) of that bridge and, as a consequence, becomes much more long-range in character. Thus, the clear distinction to the Coulombic mechanism is lost. This so-called superexchange mechanism for singlet energy transfer has been shown to make a significant contribution to the energy transfer rates in several D−B−A systems, and its D−A distance as well as D−B energy gap dependencies have been studied. We here demonstrate that in a series of oligo-*p*-phenyleneethynylene (**OPE**) bridged porphyrin-based D−B−A systems with varying D−A distances the Förster and through-bond (superexchange) mechanisms both make considerable contributions to the observed singlet energy transfer rates. The donor is either a zinc porphyrin or a zinc porphyrin with a pyridine ligand, and the acceptor is a free base porphyrin. By comparison to a homologous series where only the D−B energy gaps varies, a separation between the two energy transfer mechanisms was possible and, moreover, an interplay between distance and energy gap dependencies was noted. The distance dependence was shown to be approximately exponential with an attenuation factor $\beta = 0.20$ Å^{-1}. If the effect of the varying D−B energy gaps in the **OPE** series was taken into account, a slightly higher β-value was obtained. Ground-state absorption, steady-state, and time-resolved emission spectroscopy were used. The experimental study is accompanied by time-dependent density functional theory (TD-DFT) calculations of the electronic coupling, and the experimental and theoretical results are in excellent qualitative agreement (same distance dependence).

Introduction

Excitation energy transfer has been studied for many years with the long time goal of developing molecular scale electronics[1−5] and construction of artificial photosynthesis systems.[6−9] To systematically study energy transfer molecular donor−bridge−acceptor (D−B−A) systems have been developed and energy transfer rates as a function of bridge length,[10−18] conformation,[19] and electronic properties[20,21] have been investigated.

The electronic coupling for energy transfer can be approximated as the sum of two terms, one that describes the Coulombic interaction and one that describes the electron exchange interaction.[22−25] The two terms are active at different length scales; the electron exchange interaction, which is described by Dexter,[26] requires an orbital overlap and is therefore active at distances less than 10 Å. The Coulombic interaction, which is described by Förster,[27,28] is active at longer distances up to 100 Å. In both theories the bridge is considered as an inert spacer. In 1961 McConnell[29] derived the superexchange theory for electron transfer which also has been applied to energy transfer. According to the superexchange theory the electronic coupling between donor and acceptor can be expressed as

$$V_{DA} = \frac{V_{DB}V_{BA}}{\Delta E_{DB}} \quad (1)$$

that is, both the electronic couplings between the bridge and the donor and the acceptor (V_{DB} and V_{BA}) and the energy splitting between relevant states of the donor and bridge (ΔE_{DB}) are involved. Similar to other phenomena related to the exchange interaction, the superexchange coupling is believed to decay exponentially with distance:

$$V_{DA} = A_0 \exp\left(-\frac{\beta}{2}R_{DA}\right) \quad (2)$$

Here R_{DA} is the distance between donor and acceptor and β is the so-called attenuation factor, which usually is considered to be bridge specific. More groups than can be mentioned here have studied the distance dependence[10−18] for either singlet or triplet energy transfer, but only a few have studied the dependence on the energy splitting between donor and bridge

* Corresponding author. Phone: +46 31 772 30 44. Fax: +46 31 772 38 58. E-mail: balb@chalmers.se.
[†] Department of Physical Chemistry.
[‡] Permanent address: Research Institute for Chemistry, V.N. Karazin Kharkov National University, 4 Svobody Square, 61077 Kharkov, Ukraine.
[§] Department of Organic Chemistry.

10.1021/jp053819d CCC: $33.50
Published on Web 12/08/2005

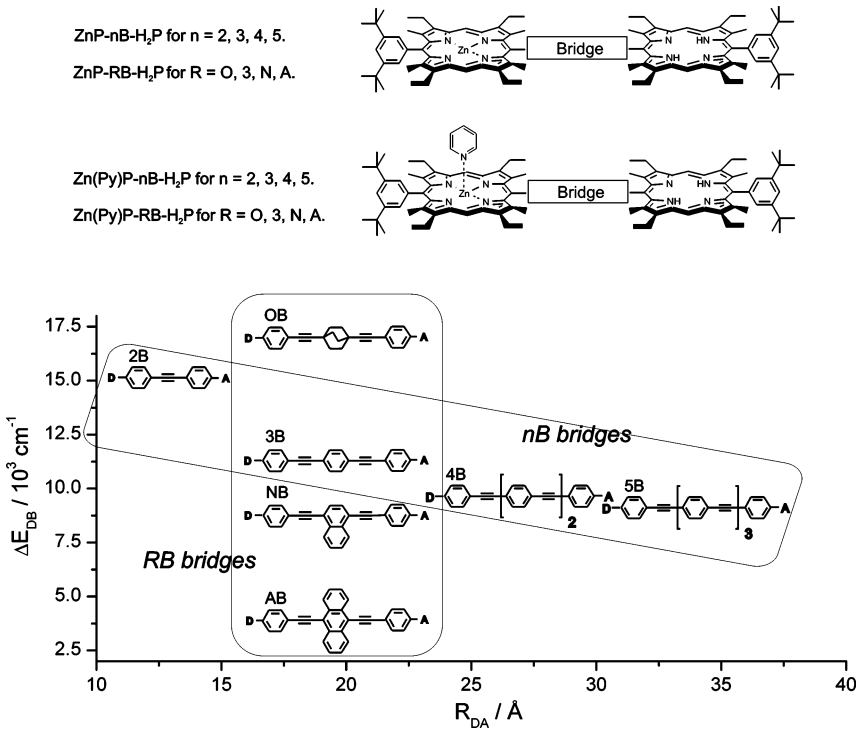

Figure 1. Structures of the dimers **ZnP−nB−H$_2$P** and **Zn(Py)P−nB−H$_2$P** compared to the structures of the earlier studied **ZnP−RB−H$_2$P** and **Zn(Py)P−RB−H$_2$P** dimers. In the energy−distance diagram the **nB** and **RB** bridges are positioned at its corresponding $\Delta E_{DB} - R_{DA}$ coordinates. ΔE_{DB} is the energy splitting between the singlet excited states of donor and bridge, and R_{DA} is the edge to edge distance between the donor (D) and acceptor (A).

(ΔE_{DB}).[20,21] We have developed two sets of porphyrin-based systems, one **ZnP−RB−H$_2$P**, where the electronic properties of the bridges are varied and the length of the bridges are kept constant, and one **ZnP−nB−H$_2$P**, where the bridge length is varied; see Figure 1. These two systems have one bridge in common, namely **3B**; this gives us the possibility to study the bridge energy and length dependence simultaneously for the first time. Our long time goal is to understand how the bridge influences the interaction between donor and acceptor for different transfer mechanisms.[20,30,31]

The D−B−A systems consist of a zinc(II) 5,15-diaryl-2,8,-12,18-tetraethyl-3,7,13,17-tetramethylporphyrin (**ZnP**) or the corresponding zinc porphyrin with a pyridine ligand (**Zn(Py)P**) as donors and the corresponding free base porphyrin (**H$_2$P**) as the acceptor. The four **RB** bridges are 1,4-bis-(phenylethynyl)bicyclo[2.2.2]octane (**OB**), 1,4-bis(phenylethynyl)benzene (**3B**), 1,4-bis(phenylethynyl)naphthalene (**NB**), and 9,10-bis(phenylethynyl)anthracene (**AB**). The **nB** bridges are a series of oligo-*p*-phenyleneethynylene (**OPE**) bridges, namely **2B**−**5B**, where $n = 2-5$ represent the number of phenyl units.

It has been shown for the **ZnP−RB−H$_2$P** and the **Zn(Py)P−RB−H$_2$P** systems that the rate constant for energy transfer varied within the series.[20,32] The differences of the measured energy transfer rates could be attributed to the "mediation effect" of the bridges, because the Förster contributions were equal within the series as the center to center distances were constant, $R_{cc} = 26.5$ Å.[33] This "mediation effect" was assigned to the superexchange mechanism because it was concluded that the rate constant for bridge mediation was strongly correlated to the inverse squared energy splitting, ΔE_{DB} (eq 1).[20] For instance, the **OB** bridge with the largest energy splitting between the singlet excited states of the donor and bridge, $\Delta E_{DB} = 17\,600$ cm^{-1}, did not enhance the energy transfer rate; that is, the rate constant was almost equal to the calculated Förster rate constant. Whereas the other three bridges, **3B**, **NB**, and **AB** with $\Delta E_{DB} = 11\,600$, 8600, and 3900 cm^{-1} respectively, substantially enhanced the rate and showed a systematic variation with the bridge−donor energy gap.

Now we want to thoroughly investigate the length and the bridge energy dependence by studying the **ZnP−RB−H$_2$P** and the **ZnP−nB−H$_2$P** systems at the same time. Both photophysical experimental results and time-dependent density functional theory (TD-DFT) calculations will be discussed.

Materials and Methods

All measurements were made at room temperature. All solvents toluene, chloroform ($CHCl_3$), and butyronitrile (C_3H_7-CN) were of analytical grade and used as purchased. The syntheses of the **ZnP−nB−H$_2$P** systems as well as the relevant reference compounds are described elsewhere.[34] The **Zn(Py)P−nB−H$_2$P** systems were prepared directly before the spectroscopic measurements by adding pyridine to the corresponding **ZnP−nB−H$_2$P** solution. Full conversion from **ZnP** to **Zn(Py)P** was obtained in an approximately 2 M pyridine solution as judged from the changes in the absorption spectra (Figure 2).

Ground-state absorption spectroscopy was performed with a Cary 4 Bio spectrophotometer or a Jasco V-530 spectrophotometer. A ground-state absorption spectrum of all samples was recorded prior to all other measurements to establish the quality of the sample and to determine its absorbance.

Steady-State Fluorescence Spectroscopy. The fully corrected emission spectra were recorded with a SPEX Fluorolog 3 or a SPEX Fluorolog τ2 spectrofluorometer. The absorbance at the excitation wavelength was kept low, approximately 0.05 (corresponding to a concentration of approximately 2.5 μM), to avoid inner filter effects and intermolecular interactions. The systems were excited at the maximum of the donor Q-band absorption (537−551 nm, depending on solvent and coordinating species).

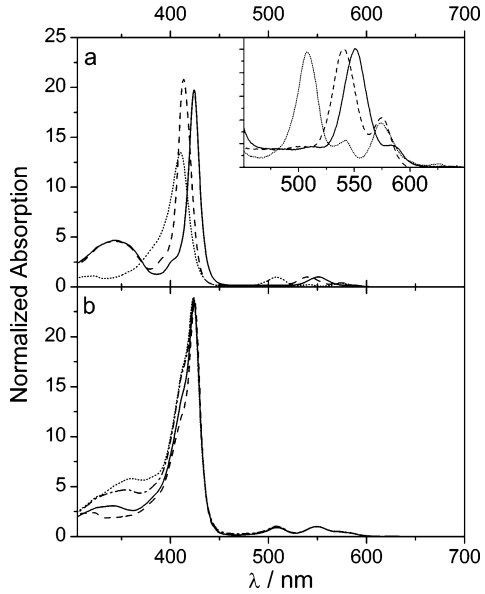

Figure 2. (a) Absorption spectra of **Zn(Py)P−4B** (—), **ZnP-4B** (---), and **H_2P** (▪▪▪) in $CHCl_3$. Inset: Q-band region magnified. (b) Absorption spectra of **Zn(Py)P−5B−H_2P** (▪▪▪), **Zn(Py)P−4B−H_2P** (-▪-), **Zn(Py)P−3B−H_2P** (—), and **Zn(Py)P−2B−H_2P** (---) in $CHCl_3$. Spectra are normalized at 550 nm.

Time-resolved fluorescence spectroscopy was carried out using the time-correlated single photon counting (TCSPC) method. An optical parametric oscillator (KTP-OPO, GWU) was pumped by a picosecond Ti:Sapphire oscillator (Tsunami, Spectra Physics) that in turn was pumped by a continuous-wave frequency-doubled diode pumped Nd:YVO4 laser (Millennia Pro, Spectra Physics). The 82 MHz output from the KTP-OPO was acousto-optically modulated to 8 MHz by a pulse selector (Spectra Physics) and frequency doubled in a BBO crystal. The excitation wavelength was kept at 551 nm where the donors, **ZnP** or **Zn(Py)P**, dominate the absorption. The sample response was recorded through a polarizer at the magic angle and a monochromator set at 580−593 nm (depending on solvent and coordinating species) to record the donor **ZnP**/**Zn(Py)P** emission and at 695−698 nm (solvent dependent) to record the acceptor **H_2P** emission. The photons were collected by a microchannel plate photo multiplier tube (MCP-PMT R3809U-50, Hamamatsu) and fed into a multichannel analyzer with 4096 channels. A diluted silica sol scattering solution was used to collect the instrument response signal. Further, the collected crude decay curves were iteratively convoluted and evaluated using the software package F900 (Edinburgh Instruments). The time resolution after deconvolution was about 10 ps (fwhm). The decays were first fitted to a single-exponential model. The goodness of fit was evaluated by χ_R^2, the residuals, and visual examination of the fitted decay. If the single-exponential decay was not satisfying, a second exponential decay and possibly a third exponential decay were used to fit the data. In toluene the decay curves of the **ZnP−nB** and **Zn(Py)P−nB** systems and the **4B**- and **5B**-bridged dimers could be fitted satisfactorily to a single exponential. For the **2B**- and **3B**-bridged dimers biexponential expressions were required. The second time constant had a small preexponential factor and was equal to the unquenched **ZnP** time constant. For the $CHCl_3$ measurements an extra time constant was used, probably due to minute impurities in the solvent. In all TCSPC experiments the absorption at the excitation wavelength was set to 0.1−0.2.

For femtosecond transient absorption measurements the pump−probe technique was employed. The setup is described in detail elsewhere.[35] The sample was held in a static 1 or 2 mm path length cuvette, and the optical density at the excitation wavelength (∼545 nm) was kept at 0.4−1.

Quantum Mechanical Calculations. The electronic coupling, V_{DA}, was calculated for symmetrical model systems by using time-dependent density functional theory (TD-DFT). The electronic coupling calculations are based on the approximation in which the exciton splitting in a symmetrical dimer, ΔE, is quantitatively related to the electronic coupling, V_{DA}:

$$V_{DA} = \Delta E/2 \tag{3}$$

In this approach the lowest excited singlet state energy splitting is taken as measure of the electronic coupling, and it has been shown to be quite successful at predicting long-range bridge-mediated interactions.[36,37] The energy splitting was obtained from TD-DFT vertical S_0-S_i excitation energies.

All DFT calculations were performed using the Gaussian 98 (revision A. 9) suite of programs.[38] The geometries were obtained using Becke's three-parameter hybrid functional referred to as B3LYP and either the 3-21G or 6-31G(d,p) basis sets. The vertical singlet-state excitation energies were calculated using the time-dependent density functional response theory[39] at the B3LYP/3-21G level. A number of vertical excitation energies were calculated at a higher level of theory, B3LYP/6-31G(d,p), to check that there was no essential basis set dependence.

Results

This section is divided into two major parts; first experimental results such as the ground-state properties, emission properties, the Förster energy transfer contribution to the donor emission, and the estimation of the rate constant for excitation energy transfer are presented. Second we present computational estimations of the electronic coupling for singlet energy transfer and studies of the relationship between the total electronic coupling and the dihedral angel between the porphyrin ring and the first phenyl unit of the bridge as well as the bridge conformation.

Experimental Results

Ground-State Absorption Properties. In Figure 2a the ground-state absorption of the reference compounds **ZnP−4B**, **Zn(Py)P−4B**, and **H_2P** are shown. Adding pyridine, which binds to the zinc porphyrin, to a **ZnP** solution red-shifts the porphyrin spectra and changes the relative intensities of the Q-bands (450−650 nm region); see inset in Figure 2a. All the **nB** bridges absorb below 400 nm, and the resulting influence on the porphyrin spectra is seen in Figure 2b. The sums of the reference compounds absorption spectra are identical with the dimers absorption spectra, which indicate that the chromophores are electronically separated; that is, the donor, bridge, and acceptor identities are preserved in the dimers. The comparatively high excitation energies of the bridges result in donor−bridge energy differences in excess of 8000 cm^{-1} (1 eV) which prevents contribution from a hopping (via the bridge) mechanism. The energy splitting ΔE_{DB} is defined as the difference in excitation energy between the bridge and donor chromophores. Experimentally the excitation energies for both the **OPE** bridges and the porphyrin chromophores are determined as the energy at the crossing point of the normalized emission and the absorption spectra.

Emission Properties. As parts of the **ZnP** and **H_2P** emission spectra are well separated, it is possible to follow the donor emission decrease and the acceptor emission increase due to the energy transfer process. The donor emission quenching is studied at the highest energy **ZnP** emission peak, around 590

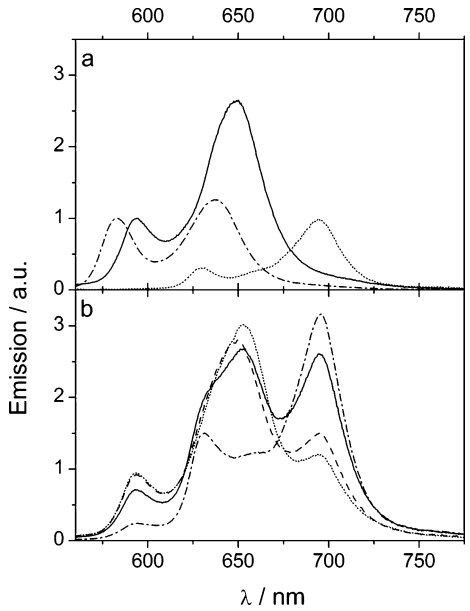

Figure 3. (a) Steady-state emission spectra of **Zn(Py)P−4B** (—), **ZnP−4B** (-·-), and **H₂P** (···) in $CHCl_3$. (b) Steady-state emission spectra of **Zn(Py)P−5B−H₂P** (···), **Zn(Py)P−4B−H₂P** (---), **Zn(Py)P−3B−H₂P** (—), and **Zn(Py)P−2B−H₂P** (-·-) in $CHCl_3$. All samples are excited at 551 nm.

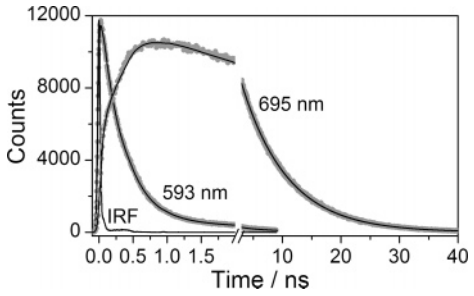

Figure 4. Fluorescence decay traces of **Zn(Py)P−2B−H₂P** in $CHCl_3$ at 593 nm, where the donor emission dominates, and at 695 nm, where the acceptor emission dominates. The solid lines are exponential fittings. IRF is the instrument response function.

nm for **Zn(Py)P** and around 580 nm for **ZnP**, and the acceptor emission increase at the lowest energy peak of **H₂P** around 700 nm (Figure 3a). The fluorescence decay traces monitored at these two peaks are shown in Figure 4. The donor emission decreases and the acceptor emission increases as the bridge length decreases, as can be seen in Figure 3b, where the emission spectra of the **Zn(Py)P−nB−H₂P** series are compared. To obtain quantitative results of the donor emission quenching, the lifetimes of the dimers, τ_{DBA} (eq 4), and reference compounds, τ_{DB} (eq 5), are compared,

$$\tau_{DBA} = (k_{ic} + k_{isc} + k_f + k)^{-1} \quad (4)$$

$$\tau_{DB} = (k_{ic} + k_{isc} + k_f)^{-1} \quad (5)$$

The quenching rate constant k (eq 6) can be calculated by assuming that the intrinsic rate constants of the donor, such as intersystem crossing (k_{isc}), internal conversion (k_{ic}), and fluorescence (k_f), are unchanged when the acceptor is introduced. The assumption is likely to hold, since the structure of the **ZnP** absorption and emission spectra does not change in the presence of **H₂P**,

$$k = (\tau_{DBA})^{-1} - (\tau_{DB})^{-1} \quad (6)$$

The rate constant is 3.4×10^9 s^{-1} for **ZnP−2B−H₂P** and decreases 2 orders of magnitude to 5.2×10^7 s^{-1} when the bridge length is increased by 20 Å (**ZnP−5B−H₂P**); see Table 1. Compared to the **ZnP−nB−H₂P** systems the rate constants for the **Zn(Py)P−nB−H₂P** systems are always smaller. For the **2B**-bridged dimers it is possible to follow the build up and decay of the acceptor **H₂P** emission; see Figure 4. The buildup time is the same as the fluorescence lifetime of the donor, and the decay time (∼9 ns) is comparable with the acceptor fluorescence lifetime.

Femtosecond transient absorption was used to investigate if electron transfer contributed to the donor quenching in any of the investigated systems. The dimer with the largest possibility for electron transfer, that is, the most quenched system **ZnP−2B−H₂P**, was studied in toluene and the more polar solvent C_3H_7CN. It was found that electron transfer can be ruled out as a major deactivation mechanism in these dimers because no evidence of radical peaks (**ZnP**$^{\bullet}$+ or **H₂P**$^{\bullet}$$^-$) could be detected in the transient absorption spectra (not show).

Förster Energy Transfer. The rate constant for energy transfer according to Förster is[27,28]

$$k_{Förster} = \frac{9000 \ln 10}{128\pi^5 N_A} \frac{\Phi_D \kappa^2 J}{\tau_D R_{cc}^6 n^4} \quad (7)$$

The quantum yield, Φ_D, and the lifetime, τ_D, of the donor are both defined in absence of the acceptor. N_A is Avogadro's number, n the refractive index of the solvent, and R_{cc} the center to center distance between donor and acceptor. The orientation factor, κ^2, describes the relative orientation of the donor and acceptor transition moments, that is, the two interacting dipoles. It has been shown that κ^2 varies between 2/3 and 1 for the different configurations of the porphyrin planes of this particular donor−acceptor system and therefore the dynamic average of 5/6 is used for κ^2 in the calculations.[20,32] Further, J is the Förster spectral overlap integral defined as

$$J = \frac{\int_0^\infty F_D(\lambda)\epsilon_A(\lambda)\lambda^4 \, d\lambda}{\int_0^\infty F_D(\lambda) \, d\lambda} \quad (8)$$

where $F_D(\lambda)$ is the fully corrected fluorescence intensity of the donor and $\epsilon_A(\lambda)$ is the acceptor molar absorptivity.

The rate constants predicted from the Förster theory are given in Table 1. The Förster contribution to the energy transfer rate is 1.5×10^9 s^{-1} for the **ZnP−2B−H₂P** system and decreases with R^{-6} to 3.2×10^7 s^{-1} for **ZnP−5B−H₂P**. The Förster energy transfer rates are significantly smaller for the **Zn(Py)P−nB−H₂P** system as the spectral overlap between donor emission and acceptor absorption is much smaller for these systems; see Table 1.

Computational Results

To theoretically model the energy transfer reactions, the electronic coupling (V_{DA}) is calculated for the model compounds in Figure 5. To simplify the calculations, symmetric D−B−D and A−B−A models of the studied D−B−A systems were used. By use of a requirement of the molecule to have at least one symmetry element (rotation axis or symmetry plane), the calculation is performed at the avoided crossing geometry and, thus, the electronic coupling could be estimated from half the energy splitting between the relevant singlet state (see Materials and Methods). Tables S1 and S2 (Supporting Information) show the electronic couplings calculated for planar bridging chro-

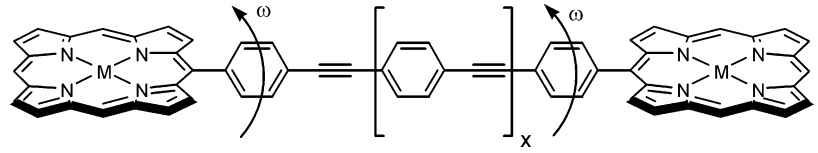

Figure 5. Structure of symmetric dimers **ZnP−nB−ZnP** (M = Zn) and **H_2P−nB−H_2P** (M = H, H; x = 0, 1, 2, 3, and 4 for n = 2, 3, 4, 5, and 6). ω is the dihedral angel between the porphyrin and phenyl rings.

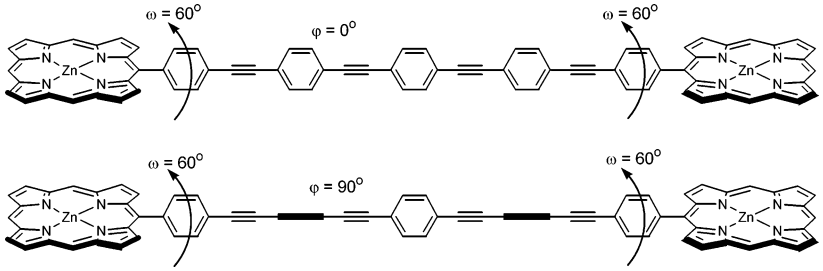

Figure 6. Two extreme conformations of **ZnP−5B−ZnP** with ω fixed at 60° and rotation of the adjacent phenyl groups an angle φ relative to each other. That is, φ = 0° means a planar bridge and φ = 90° means that adjacent phenyl groups are perpendicular to each other.

TABLE 1: Fluorescence Lifetime (τ) of the Compounds in the ZnP−nB−H_2P Series and the Reference Compounds ZnP−nB as Well as the Corresponding Pyridine Complexes in $CHCl_3$[a]

	τ (ns)	E[b]	k (s^{-1})	$k_{Förster}$ (s^{-1})	k_{med}[c] (s^{-1})	R_{ee}[d] (Å)	R_{cc}[d] (Å)	ΔE_{DB}[e] (cm^{-1})
ZnP−2B	1.27 ± 0.02							
ZnP−2B−H_2P	0.24 ± 0.01	0.81	3.4×10^9	1.5×10^9	1.9×10^9	12.7	19.7	15 800
ZnP−3B	1.29 ± 0.02							
ZnP−3B−H_2P	0.80 ± 0.02	0.38	4.7×10^8	2.5×10^8	2.2×10^8	19.6	26.5	11 600
ZnP−4B	1.28 ± 0.02							
ZnP−4B−H_2P	1.08 ± 0.01	0.16	1.4×10^8	6.2×10^7	8.2×10^7	26.5	33.4	9 700
ZnP−5B	1.28 ± 0.02							
ZnP−5B−H_2P	1.20 ± 0.01	0.06	5.2×10^7	2.0×10^7	3.2×10^7	33.4	40.3	8 800
Zn(Py)P−2B	1.19 ± 0.02							
Zn(Py)P−2B−H_2P	0.28 ± 0.01	0.76	2.7×10^9	4.0×10^8	2.3×10^9	12.7	19.7	16 100
Zn(Py)P−3B	1.19 ± 0.02							
Zn(Py)P−3B−H_2P	0.84 ± 0.10	0.29	3.5×10^8	6.8×10^7	2.8×10^8	19.6	26.5	12 000
Zn(Py)P−4B	1.19 ± 0.02							
Zn(Py)P−4B−H_2P	1.09 ± 0.03	0.08	7.7×10^7	1.7×10^7	6.0×10^7	26.5	33.4	10 000
Zn(Py)P−5B	1.18 ± 0.02							
Zn(Py)P−5B−H_2P	1.12 ± 0.02	0.05	4.5×10^7	5.5×10^6	4.0×10^7	33.4	40.3	9 100

[a] The Efficiency for the donor emission quenching (E), donor emission rate constant (k), Förster energy transfer rate constant ($k_{Förster}$), mediation rate constant (k_{med}), edge to edge (R_{ee}), and center to center (R_{cc}) distances as well as the energy difference between the singlet excited states of the donor and bridge (ΔE_{DB}). [b] $E = 1 - \tau_{DBA}/\tau_{DB}$. [c] $k_{med} = k - k_{Förster}$. [d] Distances determined from the DFT B3LYP/6-31G*-optimized structures; see Eng at al.[40] [e] The energy splitting, ΔE_{DB}, is determined from the difference in excitation energy between the bridge and donor chromophore.

mophores of different lengths. As has been noted before,[37] V_{DA} depends strongly on the dihedral angle, ω, between the bridge and porphyrin planes. The experimentally investigated systems have methyl groups at the α carbons which cause the average dihedral angle between the porphyrin and phenyl planes, ω, to be close to 90° (Figure 1). At room temperature, estimations based on a ground-state-calculated (B3LYP/6-31G*) potential surface for twisting the phenyl plane (i.e. the bridge) relative to the porphyrin plane show that conformations with ω between 60 and 120° are thermally accessible. To quantitatively compare the electronic coupling for the computationally and experimentally investigated systems, an averaging procedure needs to be employed where the different conformations should be weighted with their Boltzmann factors. In addition, the electronic coupling also depends on the conformation of the bridge (i.e. phenyl−phenyl dihedral angles), and consequently, these degrees of freedom need to be averaged as well. Rather than going through the quite tedious algebra for the averaging procedure in this paper,[41] we will make comparisons with individual conformations and the absolute magnitude of the coupling will not be discussed thoroughly. As will be seen below, qualitative results such as the distance dependence could be captured with this strategy.

TABLE 2: Electronic Couplings (V_{DA}) in the Symmetric Dimer ZnP−nB−ZnP (ω = 60°), with Different Bridge Conformations (φ) Calculated at the TD-DFT-B3LYP/3-21G Level

	V_{DA} (cm^{-1})				
Φ (deg)	**2B**	**3B**	**4B**	**5B**	**6B**
0	82.3	54.0	38.4	28.1	19.9
30	65.5	36.3	23.9	13.4	9.6
60	37.3	15.8	8.9	3.8	2.2
90	30.2	9.9	5.0	2.4	1.1
average	53.8	29.0	19.0	11.9	8.2

The calculated electronic coupling also depends quite strongly on the bridge conformation as seen in Table 2. When there is rotation of either a single phenyl group of the bridge or several at the same time always keeping at least one symmetry element (Figure 6), the value of V_{DA} varies between a maximum for the planar bridge (φ = 0°) to a minimum value for a bridge conformation where all phenyls are orthogonal (φ = 90°). Again, to reach a quantitative result these degrees of freedom need to be averaged with respect to the Boltzmann distribution, but since it is known from both experiments and quite accurate calculations that rotation of a phenyl unit in these **OPE**-bridges only requires about 1 kcal/mol, we have at this point made the

simplifying assumption that all bridge conformations are equally probable.[42,43] Using this approximation leads to the average coupling listed at the end of Table 2.

Discussion

Energy Transfer as the Dominant Deactivation Channel. Several methods independently of each other confirm that singlet energy transfer is the major deactivation channel of the excited donor. First, the acceptor emission enhancement (700 nm), in all dimers, seen in the steady-state measurements (Figure 3b) is an excellent indication of energy transfer. Second, the time constant for formation of the acceptor excited state is equal to the fluorescence lifetime of the donor, as judged from the time-correlated single photon counting measurements (Figure 4). Third, there is no evidence of radical peaks in the femtosecond transient absorption spectra, which would be expected if electron transfer was a major deactivation channel.

Comparison with Other Systems Similar to ZnP−2B−H_2P. There are examples in the literature where the **2B** bridge is used with other types of zinc and free-base porphyrins as donor−acceptor pairs, but the energy transfer rates vary largely. Lindsey and co-workers and later also Osuka and co-workers concluded that the variation is correlated to the HOMO orbitals on the specific porphyrin.[17,44] In symmetric porphyrins the two highest occupied molecular orbitals are nearly degenerate and belong to the irreducible representations A_{1u} and A_{2u} (in the D_{4h} point group). Even if the formal symmetry of the porphyrin is lower, the near degeneracy of these orbitals remain but their relative energy order depends on the peripheral substitution pattern. The A_{2u} is the HOMO orbital in tetraphenylporphyrins and has electron density at the *meso*-carbon where the bridge is attached, whereas the A_{1u}, which is the HOMO orbital in octaalkylporphyrins, has a node at the *meso* position. Accordingly, the electronic coupling through the superexchange mechanism is expected to be larger for porphyrins with electron density at the bridge attachment site (A_{2u}), and consequently, the rates are enhanced compared to porphyrins with an A_{1u} HOMO orbital. For example, a rate of 4.2×10^9 s^{-1} has been reported for a molecule similar to **ZnP−2B−H_2P** with octaalkylporphyrin A_{1u} HOMO orbitals and 10 times higher rate (4.2×10^{10} s^{-1}) for a tetraphenylporphyrin A_{2u} HOMO orbital.[17,44] These results can be compared to our measured rate for **ZnP−2B−H_2P** (3.4×10^9 s^{-1}), which has A_{1u} HOMO orbital. However, the fact that the electronic coupling is very sensitive to the bridge−porphyrin dihedral angle offers an alternative explanation to this difference. All systems reported to have "slow" energy transfer have an alkyl group at the α-carbon next to the *meso*-carbon which causes the average dihedral angle between the bridge and the porphyrin donor/acceptor to be close to 90° and according to Table 1S to have a minimal electronic coupling. In contrast, the systems with "fast" energy transfer do not have α-carbon substituents and the average bridge−porphyrin dihedral angle is close to 65° giving raise to conformations that are predicted to have much larger electronic coupling. This difference in the ground-state potential surfaces for the differently substituted porphyrins along with the sensitivity of the electronic coupling can easily explain the observed differences in energy transfer rates.

Coulombic Contribution to the Energy Transfer: Förster Energy Transfer. The Förster energy transfer contributes approximately 40−50% of the total rate constant for all the **ZnP−nB−H_2P** systems but only 10−20% in the **Zn(Py)P−nB−H_2P** systems. The large differences in Förster energy transfer rate are explained by the differences in the spectral overlap between the donor emission and the acceptor absorption. For the **ZnP−RB−H_2P** systems, we have shown that the dimer with the **OB** bridge (largest ΔE_{DB}) has a rate constant almost equal to the Förster energy transfer rate. Changing ΔE_{DB} but keeping other properties constant enhances the rate due to bridge mediated energy transfer (superexchange). The total rate constants for the **ZnP−nB−H_2P** and **Zn(Py)P−nB−H_2P** series are larger than the Förster energy transfer rate constant for all bridges; see Table 1. Still it is interesting to test the Förster theory on the data by plotting ln k versus ln R_{cc}. If the energy transfer is explained by Förster theory, the slope should be −6 according to the Förster equation (eq 7). Interestingly, as seen in Figure 7, the fitted line has a slope of −5.9.[45] Because we know that the superexchange mechanism is involved, the slope of −5.9 is a coincidence. This illustrates that obtaining a slope of −6 in a ln k versus ln R plot is not a reliable proof of the Förster mechanism.

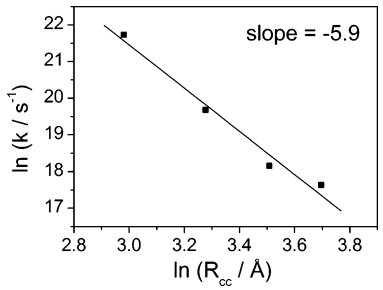

Figure 7. Logarithmic plot of k versus the center to center distance (R_{cc}) for the **Zn(Py)P−nB−H_2P** series in $CHCl_3$. The solid line is a linear fit with slope −5.9.

Superexchange Coupling: Bridge Mediation of Energy Transfer. To investigate the superexchange energy transfer rate dependence on length and ΔE_{DB}, the Förster energy transfer rate is subtracted from the total rate constant giving what we have chosen to call the mediation rate constant,

$$k_{med} = k - k_{Förster} \tag{9}$$

Since energy transfer was shown to dominate the donor quenching, the mediation rate constant, k_{med}, includes contributions from energy transfer processes that are not described by the direct dipole−dipole interaction (Förster). From the observed energy and distance dependence (vide infra), we suggest that this mediation contribution is dominated by the through-bond superexchange coupling. Other Coulomb terms such as higher multipole and through-bridge-relayed Coulombic interactions[33] might influence the rate, but the estimations based on the quantum mechanical calculations shown below suggest they have little influence. It has been shown for the **ZnP−RB−H_2P** system that k_{med} is inversely proportional to the quadratic energy splitting between the singlet excited states of the donor and bridge (ΔE_{DB}) in accordance with the superexchange mechanism. It was also shown that the magnitude of k_{med} was similar for each bridge unit in the **ZnP−RB−H_2P** and **Zn(Py)P−RB−H_2P** series; that is, a given bridge molecule adds a constant contribution to the total energy transfer rate.[20] The same conclusions holds for the **ZnP−nB−H_2P** and **Zn(Py)P−nB−H_2P** systems, and the magnitude of k_{med} for a given bridge molecule is similar; see Table 1.

Damping Factor β as an Empirical Parameter. The electronic coupling for superexchange is approximately decaying exponentially with distance; thus, the rate constant ($k \propto |V|^2$) is generally described with the following expression (cf. eq 2):

$$k = A \exp(-\beta R_{DA}) \quad (10)$$

Here β is the attenuation factor and R_{DA} is the center to center or edge to edge donor−acceptor distance. Fitting a linear function to $\ln(k_{med})$ vs R_{ee} (edge to edge distance) yields $\beta = 0.20$ Å^{-1}; see Figure 8a.[46] However, since we know that the rate of singlet excitation energy transfer also has marked donor−bridge energy gap dependence, it is interesting to investigate how this might affect the transfer rate in the series with varying length. To compensate for the varying energy gap in a series of D−B−A molecules a simple extension of eq 10 is suggested (cf. eqs 1 and 2)

$$k = \frac{\alpha}{\Delta E_{DB}^2} \exp(-\beta R_{DA}) \quad (11)$$

where the preexponential factor has been made bridge energy dependent according to the experimentally verified superexchange mechanism for the systems with constant D−A distance (the **RB** series). In Figure 8b a linearized version of eq 11 is plotted against the edge to edge distance (the experimentally determined ΔE_{DB} values are found in Table 1) and fitted to a line with slope $\beta = 0.25$ Å^{-1} and intercept $\ln \alpha = 43.5$. The fit compared to Figure 8a is not improved much but enables a comparison with the results from a fit in the energy gap dimension. In Figure 8c the energy transfer rate constants from measurements on the **ZnP**−**RB**−**H$_2$P** and **Zn(Py)P**−**RB**−**H$_2$P** series[20] are plotted against $\Delta E_{DB}{}^{-2}$ and fitted to a straight line, which from eq 11 is expected to have a slope of $\alpha \exp(-\beta R_0)$, where $R_0 = 19.6$ Å is the constant donor−acceptor separation in the **RB** series. Now, if we use $\beta = 0.25$ Å^{-1} as found from fitting the **nB** series data, it is possible to calculate the parameter α also from the slope in Figure 8c, and this yields $\ln \alpha = 42.2$. This is a quite reasonable result when comparing the two sets of measurements giving strength to the assumptions behind eq 11. It should be noted that the energy in eq 11 is different from the constant energy gap normally discussed in the superexchange mechanism. Equation 11 gives the approximate rate expected for excitation energy tunneling through a rectangular barrier with height ΔE_{DB} and width R_{DA}.

The attenuation factor is usually regarded to be a bridge specific parameter, and it could be interesting to compare the magnitude of β found in this study with those for similar π-conjugated bridges. Others have reported for energy transfer $\beta = 0.32$ Å^{-1} and $\beta = 0.33$ Å^{-1} for phenylene bridges,[13,15] $\beta = 0.17$ Å^{-1} for alkyne bridges,[14] and $\beta = 0.11$ Å^{-1} for dialkoxy-substituted **OPE** bridges.[16] When we compare these β-values, it must be remembered that they have not been "compensated" for the donor−bridge energy dependence and a comparison is therefore only meaningful for D−B−A system with similar donor−bridge energy gaps.

Calculations of the Electronic Coupling for Singlet Energy Transfer: Porphyrin−Bridge Conformations. The distance dependence of the calculated electronic coupling could be analyzed in the same way as the experimental distance dependence. In Figure 9 the logarithm of $V_{DA}{}^2$ for planar bridges is plotted against the edge to edge distance, R_{ee}. As expected, the electronic coupling shows an exponential falloff with distance with a slope that is independent of the bridge−porphyrin dihedral angle, ω. The attenuation factor, β, is 0.10 Å^{-1} for the **ZnP**−**nB**−**ZnP** series and 0.12 Å^{-1} for the **H$_2$P**−**nB**−**H$_2$P** series. These β-values are substantially smaller than the experimentally determined ones, and there are two obvious reasons for this discrepancy. First, the bridge in reality is not planar but adopts many nonplanar conformations. Second, the calculated porphyrin−bridge energy gaps, ΔE_{DB}, are consistently smaller than the experimental gaps, which also are expected to yield smaller attenuation factors. Both these factors are discussed below.

Calculations of the Electronic Coupling for Singlet Energy Transfer: Bridge Conformations. The electronic coupling has been shown to be strongly dependent on the bridge conformation in a number of studied D−B−A systems.[37,47] It is therefore important to analyze how the distance dependence is influenced

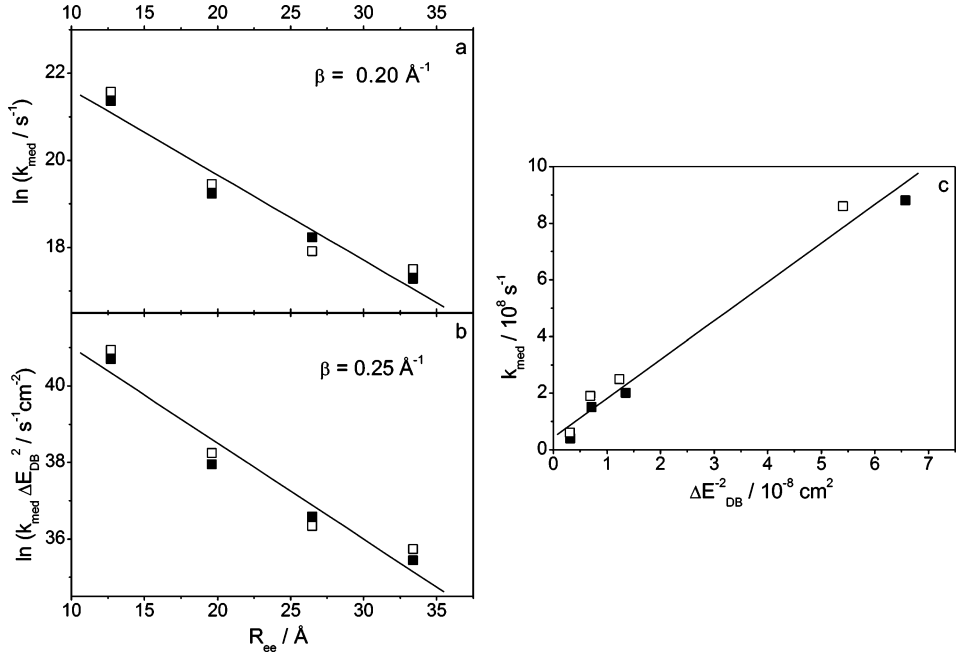

Figure 8. (a) Semilogarithmic plot of k_{med} versus the edge to edge (R_{ee}) distance for the **ZnP**−**nB**−**H$_2$P** (■) and the **Zn(Py)P**−**nB**−**H$_2$P** (□) series in $CHCl_3$. The solid line shows the best linear fit to eq 10. (b) Semilogarithmic plot of $(k_{med})(\Delta E_{DB}{}^2)$ versus the edge to edge (R_{ee}) distance for the **ZnP**−**nB**−**H$_2$P** (■) and the **Zn(Py)P**−**nB**−**H$_2$P** (□) series in $CHCl_3$. The solid line shows the best linear fit to eq 11. (c) Plot of k_{med} vs $\Delta E_{DB}{}^{2-}$ for the **ZnP**−**RB**−**H$_2$P** (■) and **Zn(Py)P**−**RB**−**H$_2$P** (□) series in $CHCl_3$. The solid line shows the best linear fit to eq 11 with $R_{DA} = R_0 = 19.6$ Å (adopted from ref 20).

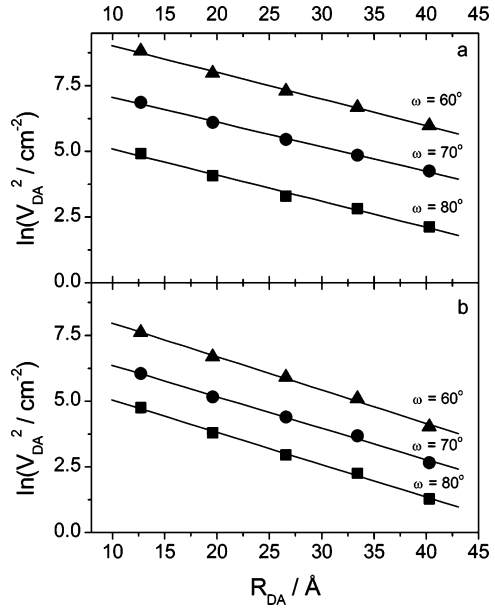

Figure 9. Semilogarithmic plot of TD-DFT-B3LYP/3-21G-calculated V_{DA}^2 versus the edge to edge donor−acceptor distance (R_{ee}) for different dihedral angles (ω). The bridge is kept planar. Key: (a) symmetric **ZnP**−**nB**−**ZnP** dimer; (b) symmetric **H₂P**−**nB**−**H₂P** dimer.

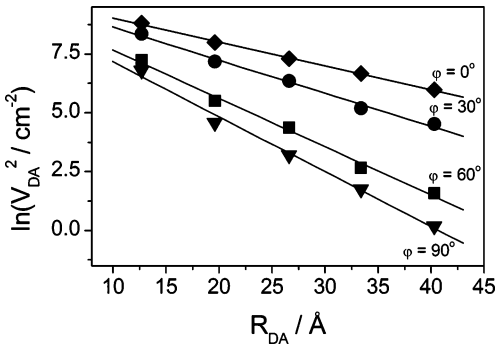

Figure 10. Semilogarithmic plot of the TD-DFT-B3LYP/3-21G-calculated V_{DA}^2 versus the edge−edge donor acceptor distance for the symmetric **ZnP**−**nB**−**ZnP** dimer with $\omega = 60°$ and with different bridge conformations $\varphi = 0°$ (diamonds) and $\beta = 0.10$ Å^{-1}, $\varphi = 30°$ (circles) and $\beta = 0.14$ Å^{-1}, $\varphi = 60°$ (squares) and $\beta = 0.21$ Å^{-1}, and $\varphi = 90°$ (triangles) and $\beta = 0.23$ Å^{-1}. The averaged electronic coupling assuming equal weight of all bridge conformations yields $\beta = 0.14$ Å^{-1}.

by allowing the bridge to adopt nonplanar conformations. In Figure 10 the calculated electronic coupling is shown for four representative bridge conformations. It is clearly seen that the β-factor varies systematically with the dihedral angle, φ. The nonplanar bridges show a faster falloff than the planar with β-factors varying between 0.10 Å^{-1} (planar) and 0.23 Å^{-1} (orthogonal phenyl planes). This is a smaller variation than has been noted before in calculations of electron transfer through **OPE** bridges[47] and also for triplet energy transfer.[40] The small variation in β between planar and nonplanar bridge conformations might be due to direct Coulombic contributions to the calculated electronic coupling which is possible for long-range singlet energy transfer but not for triplet energy transfer or electron transfer. Therefore, the direct Coulombic interaction between the porphyrins in the model compounds was estimated with the same computational method. By removal of the bridge and keeping the porphyrins at the same distance and orientation, an accurate estimate of the Coulombic contribution is expected. This direct mechanism is, somewhat surprisingly when comparing to the experimental reality, calculated to make a very small relative contribution to the total coupling (less than 1% at all distances). The explanation to this is, however, quite straightforward. In the TD-DFT calculations the magnitudes of the electronic transition dipole moments for the porphyrins are dramatically underestimated, which leads to the leading dipole−dipole contribution to the Coulombic interaction being underestimated.[48] In our qualitative analysis this is actually beneficial since we want to compare the exchange part of the electronic coupling to the non-Förster rates, k_{med}. Of course, if the absolute magnitude of the electronic coupling for singlet energy transfer is required, both the direct Coulombic and exchange contributions must be correctly calculated. In summary, direct Coulombic interaction effects could not explain the weak bridge conformation dependence on the β-factor (Figure 10).

The second obvious difference between the experimental and computational systems was that the energy gaps were underestimated in the calculations. This is easily removed by "normalizing" the rates (squared couplings) with the relevant energy gaps as was suggested in eq 11 and demonstrated in Figure 8b. If the logarithm of the calculated $V_{DA}^2 \times \Delta E_{DB}^2$ is plotted against the edge to edge distance, nice linear fits are obtained for all bridge dihedral angles (Figure S1, Supporting Information) with slopes corresponding to β-values 0.21 Å^{-1} ($\phi = 0°$), 0.25 Å^{-1} ($\phi = 30°$), 0.32 Å^{-1} ($\phi = 60°$), and 0.35 Å^{-1} ($\phi = 90°$). The agreement with the experimentally determined $\beta = 0.25$ Å^{-1} is excellent, which shows that the dominating difference between experiments and calculations in this case lies in the donor−bridge energy gap difference.

Conclusions

We have studied the donor−acceptor distance and donor−bridge energy dependence of singlet energy transfer in a series of D−B−A systems. Both experimental and theoretical methods have been used, and a consistent description of the energy-transfer process emerges from the study. In condensed form the following has been learned: (1) Singlet energy transfer occurs with both a Coulombic (Förster) and through-bond superexchange mechanism in these **OPE**-bridged porphyrin D−B−A systems. The contribution from the two mechanisms is approximately of the same magnitude, and the relative contributions do not vary with the D−A distance. (2) To understand both the D−A distance and D−B energy difference dependencies at the same time requires that the bridge energy variations are accounted for in the model. (3) The through-bond coupling for singlet energy transfer was shown to decay approximately exponentially with an experimentally determined attenuation factor of $\beta = 0.20$ Å^{-1}. (4) The decay of the theoretically calculated electronic coupling was shown to be independent of the bridge−porphyrin dihedral angle but significantly dependent on the bridge conformation (planar vs nonplanar). (5) If both the experimental and theoretical rates/couplings are normalized with the D−B energy gap (eq 11), very good agreements between the attenuation factors were obtained.

Acknowledgment. This work was supported by grants from the Swedish Research Council (VR), the Knut and Alice Wallenberg Foundation, and the Hasselblad Foundation.

Supporting Information Available: Calculated electronic couplings for the **ZnP**−**nB**−**ZnP** and **H₂P**−**nB**−**H₂P** series as a function of dihedral angle calculated at different TD-B3LYP levels and semilogarithmic plots of the TD-DFT-B3LYP/3-21G-calculated $\Delta E_{DB}^2 V_{DA}^2$ versus the edge to edge donor acceptor

distance for the symmetric **ZnP−nB−ZnP** dimer with $\omega = 60°$ and with different bridge conformations. This material is available free of charge via the Internet at http://pubs.acs.org.

References and Notes

(1) In *Molecular Electronics*; Jortner, J., Ratner, M. A., Eds.; Blackwell Science Ltd.: Oxford, U.K., 1997.

(2) Balzani, V.; Credi, A.; Venturi, M. *Chem. Phys. Chem.* **2003**, *4*, 49−59.

(3) Balzani, V. *Photochem. Photobiol. Sci.* **2003**, *2*, 459−476.

(4) Ball, P. *Nature* **2000**, *406*, 118−120.

(5) Burrell, A. K.; Wasielewski, M. R. *J. Porphyrins Phthalocyanines* **2000**, *4*, 401−406.

(6) Gust, D.; Moore, T. A.; Moore, A. L. *Acc. Chem. Res.* **2001**, *34*, 40−48.

(7) Sun, L. C.; Hammarström, L.; Åkermark, B.; Styring, S. *Chem. Soc. Rev.* **2001**, *30*, 36−49.

(8) Moore, T. A.; Moore, A. L.; Gust, D. *Philos. Trans. R. Soc. London, Ser. B* **2002**, *357*, 1481−1498.

(9) Wasielewski, M. R. *Chem. Rev.* **1992**, *92*, 435−461.

(10) Zimmerman, H. E.; Goldman, T. D.; Hirzel, T. K.; Schmidt, S. P. *J. Org. Chem.* **1980**, *45*, 3933−3951.

(11) Oevering, H.; Verhoeven, J. W.; Paddon-Row, M. N.; Cotsaris, E.; Hush, N. S. *Chem. Phys. Lett.* **1988**, *143*, 488−495.

(12) Osuka, A.; Tanabe, N.; Kawabata, S.; Yamazaki, I.; Nishimura, Y. *J. Org. Chem.* **1995**, *60*, 7177−7185.

(13) Barigelletti, F.; Flamigni, L.; Guardigli, M.; Juris, A.; Beley, M.; Chodorowski-Kimmes, S.; Collin, J.-P.; Sauvage, J.-P. *Inorg. Chem.* **1996**, *35*, 136−142.

(14) Harriman, A.; Ziessel, R. *Chem. Commun.* **1996**, 1707−1716.

(15) Schlicke, B.; Belser, P.; De Cola, L.; Sabbioni, E.; Balzani, V. *J. Am. Chem. Soc.* **1999**, *121*, 4207−4214.

(16) Harriman, A.; Khatyr, A.; Ziessel, R.; Benniston, A. C. *Angew. Chem., Int. Ed.* **2000**, *39*, 4287−4290.

(17) Cho, H. S.; Jeong, D. H.; Yoon, M. C.; Kim, Y. H.; Kim, Y. R.; Kim, D.; Jeoung, S. C.; Kim, S. K.; Aratani, N.; Shinmori, H.; Osuka, A. *J. Phys. Chem. A* **2001**, *105*, 4200−4210.

(18) Smith, T. A.; Lokan, N.; Cabral, N.; Davies, S. R.; Paddon-Row, M. N.; Ghiggino, K. P. *J. Photochem. Photobiol., A* **2002**, *149*, 55−69.

(19) Kroon, J.; Oliver, A. M.; Paddon-Row, M. N.; Verhoeven, J. W. *J. Am. Chem. Soc.* **1990**, *112*, 4868−4873.

(20) Kilså, K.; Kajanus, J.; Mårtensson, J.; Albinsson, B. *J. Phys. Chem. B* **1999**, *103*, 7329−7339.

(21) El-Ghayoury, A.; Harriman, A.; Khatyr, A.; Ziessel, R. *Angew. Chem., Int. Ed.* **2000**, *39*, 185−189.

(22) Turro, N. J. *Modern Molecular Photochemistry*; The Benjamin/Cummings Publishing Co., Inc.: Menlo Park, CA, 1978.

(23) Scholes, G. D.; Harcourt, R. D.; Ghiggino, K. P. *J. Chem. Phys.* **1995**, *102*, 9574−9581.

(24) Harcourt, R. D.; Scholes, G. D.; Ghiggino, K. P. *J. Chem. Phys.* **1994**, *101*, 10521−10525.

(25) Scholes, G. D.; Ghiggino, K. P. *J. Chem. Phys.* **1995**, *103*, 8873−8883.

(26) Dexter, D. L. *J. Chem. Phys.* **1953**, *21*, 836−850.

(27) Förster, T. *Naturwissenschaften* **1946**, *33*, 166−175.

(28) Förster, T. *Ann. Phys.* **1948**, *2*, 55−75.

(29) McConnell, H. M. *J. Chem. Phys* **1961**, *35*, 508−515.

(30) Andréasson, J.; Kajanus, J.; Mårtensson, J.; Albinsson, B. *J. Am. Chem. Soc.* **2000**, *122*, 9844−9845.

(31) Kilså, K.; Kajanus, J.; Macpherson, A. N.; Mårtensson, J.; Albinsson, B. *J. Am. Chem. Soc.* **2001**, *123*, 3069−3080.

(32) Jensen, K. K.; van Berlekom, S. B.; Kajanus, J.; Mårtensson, J.; Albinsson, B. *J. Phys. Chem. A* **1997**, *101*, 2218−2220.

(33) This was previously reported to be 25.3 Å, but more refined methods (DFT B3LYP/6-31G*) estimate the center to center distance to be 26.5 Å; see ref 40.

(34) Ljungdahl, T.; Pettersson, K.; Albinsson, B.; Mårtensson, J. Submitted for publication in *Eur. J. Org. Chem.*

(35) Pettersson, K.; Kilså, K.; Mårtensson, J.; Albinsson, B. *J. Am. Chem. Soc.* **2004**, *126*, 6710−6719.

(36) Clayton, A. H. A.; Scholes, G. D.; Ghiggino, K. P.; Paddon-Row, M. N. *J. Phys. Chem.* **1996**, *100*, 10912−10918.

(37) Kyrychenko, A.; Albinsson, B. *Chem. Phys. Lett.* **2002**, *366*, 291−299.

(38) Frisch, M. J.; Trucks, G. W.; Schlegel, H. B.; Scuseria, G. E.; Robb, M. A.; Cheeseman, J. R.; Zakrzewski, V. G.; Montgomery, J. A., Jr.; Stratmann, R. E.; Burant, J. C.; Dapprich, S.; Millam, J. M.; Daniels, A. D.; Kudin, K. N.; Strain, M. C.; Farkas, O.; Tomasi, J.; Barone, V.; Cossi, M.; Cammi, R.; Mennucci, B.; Pomelli, C.; Adamo, C.; Clifford, S.; Ochterski, J.; Petersson, G. A.; Ayala, P. Y.; Cui, Q.; Morokuma, K.; Malick, D. K.; Rabuck; Raghavachari; Foresman, J. B.; Cioslowski, J.; Ortiz, J. V.; Baboul, A. G.; Stefanov, B. B.; Liu, G.; Liashenko, A.; Piskorz, P.; Komaromi, I.; Gomperts, R.; Martin, R. L.; Fox, D. J.; Keith, T.; Al-Laham, M. A.; Peng, C. Y.; Nanayakkara, A.; Challacombe, M.; Gill, P. M. W.; Johnson, B.; Chen, W.; Wong, M. W.; Andres, J. L.; Gonzalez, C.; Head-Gordon, M.; Replogle, E. S.; Pople, J. A. *Gaussian 98*, revision A.9; Gaussian, Inc.: Pittsburgh, PA, 1998.

(39) Ditchfield, R.; Hehre, W. J.; Pople, J. A. *J. Chem. Phys.* **1971**, *54*, 724.

(40) Eng, M. P.; Ljungdahl, T.; Mårtensson, J.; Albinsson, B. Submitted to *J. Phys. Chem. B.*

(41) This averaging procedure will be discussed in a forthcoming paper; see ref 40.

(42) Levitus, M.; Schmieder, K.; Ricks, H.; Shimizu, K. D.; Bunz, U. H. F.; Garcia-Garibay, M. A. *J. Am. Chem. Soc.* **2001**, *123*, 4259−4265.

(43) Schmieder, K.; Levitus, M.; Dang, H.; Garcia-Garibay, M. A. *J. Phys. Chem. A* **2002**, *106*, 1551−1556.

(44) Strachan, J. P.; Gentemann, S.; Seth, J.; Kalsbeck, W. A.; Lindsey, J. S.; Holten, D.; Bocian, D. F. *J. Am. Chem. Soc.* **1997**, *119*, 11191−11201.

(45) The slope varies between −5.9 and −6.7 for the **ZnP−nB−H_2P** and **Zn(Py)P−nB−H_2P** systems in toluene and $CHCl_3$.

(46) The attenuation factor (β) for **ZnP−nB−H_2P** and **Zn(Py)P−nB−H_2P** is determined to 0.20 $Å^{-1}$ in $CHCl_3$ and 0.20 and 0.22 $Å^{-1}$, respectively, in toluene.

(47) Sachs, S. B.; Dudek, S. P.; Hsung, R. P.; Sita, L. R.; Smalley, J. F.; Newton, M. D.; Feldberg, S. W.; Chidsey, C. E. D. *J. Am. Chem. Soc.* **1997**, *119*, 10563−10564.

(48) Sundholm, D. *Phys. Chem. Chem. Phys.* **2000**, *2*, 2275−2281.